Highly Extensible Skin of a Variable Geometry Wing Leading Edge of a High-Performance Sailplane

Matthias Weinzierl
matthias.weinzierl@tum.de

Johannes Achleitner
johannes.achleitner@tum.de

Horst Baier
baier@tum.de

Institute for Lightweight Structures
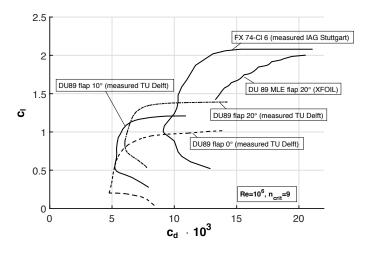*Technische Universität München*
Munich, Germany

Abstract

In 2011 the Akaflieg München e.V. began research on a variable geometry wing of a sailplane. The advantage of a leading edge with a variable camber was investigated by Wießmeier on the basis of the ASW 27 airfoil. The results show a great potential of achieving a higher wing loading and a higher cruising speed along with excellent low-speed flight characteristics. Subsequently, different designs of the technical implementation of a variable geometry wing leading edge are considered. This paper presents the results of a study whose principal aim is to design and analyse a highly extensible section of a variable geometry wing leading edge. This section is designed as a sandwich, composed of an accordion honeycomb core with elastomeric top layers. It has a high bending stiffness as well as a high extensibility into one direction, allowing for the wing leading edge to morph downward.
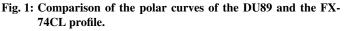
Nomenclature

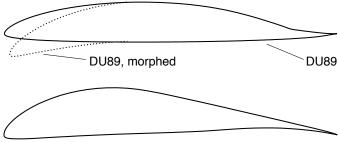|	
c_d	Drag coefficient of the profile
c_l	Lift coefficient of the profile
C_{D_i}	Induced drag coefficient of the wing
C_L	Lift coefficient of the wing
el	Distance between two cells
h	Distance between two bars
h_{bar}	Height of the bar
h_{core}	Height of the core
k	Induced drag factor
l	Length of the bar
t	Thickness of the bar
t_h	Thickness of the cross stud
x-axis	Direction of flight
y-axis	Spanwise direction
A	Cross sectional area of the core
θ	Opening angle of the accordion
Λ	Aspect ratio

Introduction

Modern airfoils of flapped sailplanes have a laminar low drag bucket ranging from a lift coefficient of $c_l = 0.1$ to $c_l = 1.5$ [1]. For higher wing aspect ratios combined with higher wing loadings to be realized, the low drag bucket needs to be widened

towards higher lift coefficients. Liebeck, Wortmann and Selig each developed single-element high-lift airfoil designs, which show a maximum lift coefficient of around $c_l = 2.3$ [2–4]. Especially Wortmann's FX-74CL series shows very high lift coefficients of $c_l = 2.0$ combined with acceptable drag coefficients of $c_d = 13 \cdot 10^{-3}$ in the upper end of the laminar low drag bucket, as shown in Fig. 1. A possible solution for the widening of the low drag bucket is shown by Wießmeier with a profile derived

Fig. 1: Comparison of the polar curves of the DU89 and the FX-74CL profile.

Fig. 2: Comparison of the DU89 profile, the morphed DU89 and the FX-74CL.
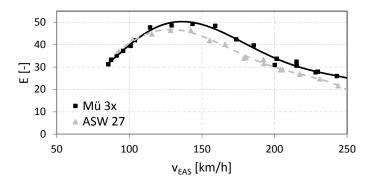

Fig. 3: Comparison of the glide ratio of the ASW 27 versus the Mü 3x at maximum take off mass (MTOM) [5].

from the DU89 profile, which is used as the main wing airfoil of the ASW 27. A comparison of the FX-74CL, the DU89 and the morphed version of the DU89 by Wießmeier can be seen in Fig. 2 [5]. The upper end of the laminar low-drag bucket of the morphed version of the DU89 is at a 20% higher lift coefficient compared to the unmorphed version.

During low-speed flight a higher induced drag coefficient is caused due to higher lift coefficient, as can be seen in the following equation:

$$C_{D_i} = \frac{C_L^2}{\pi \Lambda} k \tag{1}$$

This higher drag coefficient can be compensated by a higher aspect ratio of the wing. Subsequently this higher aspect ratio and a higher wing loading have no impact on the low-speed performance but lead to an excellent performance within and above the range of the best glide ratio, compared to modern flapped sailplanes. Wießmeier estimated an empty weight of the morphing wing aircraft increased by 45 kg compared to that of the ASW 27 [5]. However, he pointed out that a higher mass is not necessarily a disadvantage, due to the fact that the morphing wing aircraft has limited water ballast capacity.

A polar of a sailplane with a variable geometry leading edge can be calculated by subtracting the profile drag and the induced drag from a known total drag polar of the sailplane. This results in a fuselage drag, an interference drag and a tailplane drag. By adding the envelope of the profile drag of the new profile with

the variable geometry leading edge to the induced drag of the new wing calculated in Eq. 1, a theoretical polar of the new sailplane has been achieved. Although this way of calculating the polar is an approximation due to neglecting different profile sections on the wing and different interference drags, an estimation of the gain in performance could be given. Wießmeier showed a remarkable performance improvement using his new profile and a wing with a surface area reduced by 20% compared to the ASW 27, as can be seen in Fig. 3. The data of the DU89 and the FX-74CL have been measured at TU Delft and IAG Stuttgart whereas the data of the DU89MLE have been calculated with *XFOIL*. Concerning maximum lift and performance at high lift coefficients, *XFOIL* significantly overestimates airfoil performance in some cases [6–10]. A comparison between the lift coefficient of the DU89 calculated with *XFOIL* and the one measured at TU Delft is shown in Fig. 4. In the calculation with 0° flaps *XFOIL* overestimates the lift coefficient by approximately 8% while in the calculation with 20° flaps *XFOIL* underestimates the lift coefficient by approximately 3%. In further research, an airfoil optimized for a morphing wing should be designed and verified with wind tunnel tests.

For commercial aircraft, the "Deutsches Zentrum für Luft- und Raumfahrt" (DLR), investigates different drop nose and morphing trailing edge concepts [11–17]. These drop nose concepts are based on a widespread extension in the entire leading edge, which is designed of fiberglass. The DLR has built several demonstrators of their drop nose concepts and now attempts to implement the design in an aircraft.

In 1978, Burkhart Grob Luft- und Raumfahrt GmbH developed the 15 meter class sailplane "G104 Speed Astir," which can be seen as a pioneer in morphing wing design. The flaperons were designed as elastic flaps, which reduce the drag otherwise created by the gap between the trailing edge and the flap. The skin in this area is highly flexible around the *y*-axis [18].
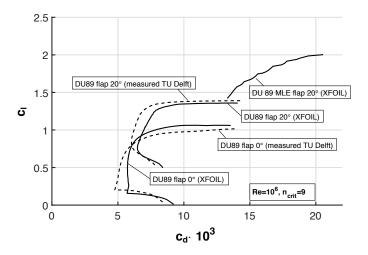

Fig. 4: Comparison of the calculated and the measured polar curves of the DU89.
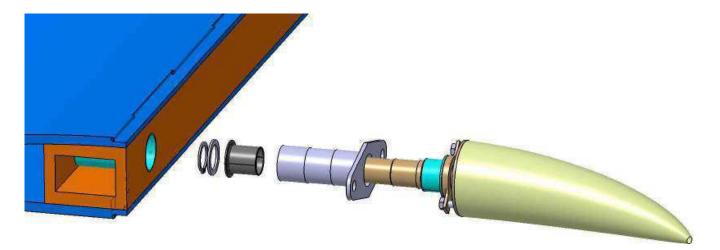
Fig. 5: Rotary Drive System (RDS) with horns [5].

Structural-mechanical implementation of a variable geometry leading edge

The technical implementation of the variable geometry leading edge represents a challenge. Wießmeier suggested a Rotary Drive System (RDS) with multiple horns to morph the leading edge down, which can be seen in Fig. 5 [5]. These horns are placed in front of the wing spar. Turning the horn changes the contour of the leading edge surface. The first contour is the one of the non-cambered leading edge while the second contour is the one of the fully cambered leading edge. This second contour is turned by 90° compared to the non-cambered one. By turning the horns, the profile can be cambered from the original shape to a high-lift contour. This leads to a high extension in the upper shell of the wing. In the late 1990s the RDS concept for a morphing trailing edge was extensively researched by Müller [19]. He reached a technology readiness level of 4 by accomplishing a full scale demonstrator, which reached a deflection of the trailing edge of ±15°. In the following paragraph an approach is presented, using a highly extensible section designed in a sandwich construction and placed in front of the main spar.
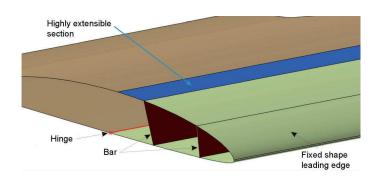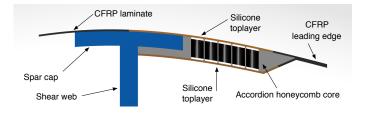

Fig. 6: Highly extensible section [20].

Fig. 7: Connection of the highly extensible section to the fixed shape leading edge [21].

Highly extensible section

One possible solution to implement a morphing leading edge with a RDS is the use of a highly extensible section placed in front of the main spar in the upper shell of the wing, as shown in Figs. 6 and 7.

This version with the highly extensible section splits the leading edge in two different parts: The main part approximately keeps its original shape while the highly extensible section becomes severely deformed. The requirements on this highly extensible section are on the one hand an extensibility of 30% in the direction of flight (*x*-direction) and a low bending stiffness around the *y*-axis (spanwise direction) [20]. On the other hand the highly extensible section needs a high bending stiffness around the *x*-axis to withstand the aerodynamic loads [21].

For achieving such a highly extensible section, a sandwich structure with anisotropic material parameters seems to be a possible solution. Therefore, a core without lateral contraction can be combined with elastomeric top layers. A core without any lateral contraction and a high extensibility in the *x*-direction is called a zero-Poisson honeycomb core or an accordion honeycomb core [22, 23]. The geometrical parameters of such a honeycomb core are shown in Fig. 8.

In a parametric study different combinations of the geometrical parameters of the accordion honeycomb core are investigated and compared with each other. The goal of the parametric
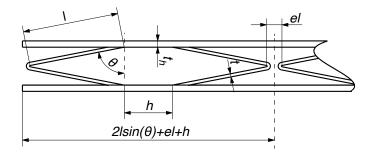
Fig. 8: Geometrical parameters of an accordion honeycomb core [24].

Table 1: Chosen parameters of the final version of the accordion honeycomb core of the Mü 3x [21].

Parameter	Value
θ	79.0°
l	16.0 mm
t	0.5 mm
h_{bar}	12.0 mm
h_{core}	10.0 mm

Fig. 9: Local strain within the accordion honeycomb core [21].

Fig. 10: Prototype of the final version of the accordion honeycomb core [21].

study is a configuration with a large ratio of global strain to local strain in the *x*-direction compared with a relatively high bending stiffness around the *x*-axis. As a final version an accordion honeycomb core with a height of 10.0 mm and a thickness of the spars of 0.5 mm is chosen. All parameters are listed in Table 1. In this configuration the local strain in the material is 0.4% while the global strain of the core is 30%. The local strain of the core is shown in Fig. 9.

With the parameters listed in Table 1 a first prototype is built, as can be seen in Fig. 10. The prototype is built by additive manufacturing and as material the polyamide PA 2200 is chosen, which is based on a PA-12. The material data of the PA 2200 from the supplier are listed in Table 2. Material data of environmental effects (e.g. moisture or temperature) are not available.

To validate the results of the Young's modulus and the strength results of the numerical calculation, the prototype is submitted to a tensile strength test. Between the measured values of the Young's modulus and the calculated ones is a difference of about 1.2%, which can be considered negligible. A linear elastic material behavior appears up to 50% global strain and the fracture strain is ca. 230%. The linear elastic material behavior can be seen in the stress-strain curve in Fig. 11. The stress gets normalized to the cross sectional area $A = [2l \sin(\theta) + el + h] \cdot h_{core}$ of the unit cell. Due to this relatively large cross section, the value of the Young's modulus becomes 0.01 MPa.
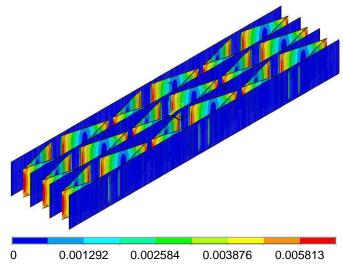
Surface layers

For achieving a smooth surface and a higher bending stiffness of the highly extensible section, top layers are needed. In a first attempt they are designed in pure silicone. Every layer has a thickness of 1.0 mm. For material the pure silicone ALPA-SIL 32 is chosen. With the first prototype two major problems occur: First the silicone detaches itself from the core material and second the lateral contraction of the silicone causes constraining forces and stress in the sandwich. To achieve a better bonding of the silicone top layers to the polyamide core, a form-fitting connection is realized, as can be seen in Fig. 12. With this improvement a second prototype of the sandwich including the accordion honeycomb core and the silicone top layers is built, as can be seen in Fig. 13.

Table 2: Material data for PA 2200 [25].

Average grain size	56	μm
Density laser sintered	0.93	g/cm^3
Tensile modulus	1700	MPa
Tensile strength	48	MPa
Elongation at break	24	%
Bending modulus	1500	MPa
Bending strength	58	MPa
Melting point	180	°C
Shore hardness D	75	[–]
Poisson's ratio	0.4	[–]

Fig. 11: Stress-strain curve of the accordion honeycomb core [21].

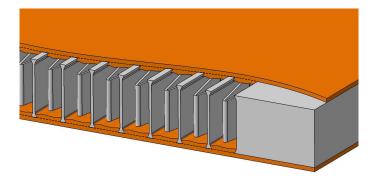**Fig. 12: Form-fitting core and top layers [21].**

Fig. 13: Sandwich with accordion honeycomb core and silicone top layers [21].

Conclusions

A morphing leading edge seems to be advantageous for a sailplane in different aspects. To implement such a leading edge, a RDS combined with a highly extensible section in the upper shell of the wing is a possible solution. The highly extensible section can be designed as a sandwich with an accordion honeycomb core with silicone top layers. This sandwich has a high extensibility in the *x*-direction without any lateral contraction. By choosing the appropriate parameters of the accordion honeycomb core, an expansion ratio of 75 between the global strain and the local strain can be achieved. The final design of the accordion honeycomb core fulfills all requirements on the core structure. In further studies the material behavior of top layers should be characterized as well as the bonding of the top layers to the core structure. The use of fiber-reinforced elastomers as top layers could also prove advantageous.

References

[1] Boermans, L., "Research on Sailplane Aerodynamics at Delft University of Technology," *Technical Soaring*, Vol. 30, No. 1/2, 2006.

[2] Liebeck, R. and Ormsbee, A., "Optimization of airfoils for maximum lift," *Journal of Aircraft*, Vol. 7, No. 5, Sept. 1970, pp. 409–416.

[3] Althaus, D., *Niedriggeschwindigkeitsprofile*, Vieweg Verlag, 1996.

[4] Selig, M. and Guglielmo, J., "High-Lift Low Reynolds Number Airfoil Design," *Journal of Aircraft*, Vol. 34, No. 1, Jan. 1997, pp. 72–79.

[5] Wießmeier, M., *Konzept einer formvariablen Tragflügelvorderkante bei einem Segelflugzeug mit innenliegender Ansteuerung über ein Rotary Drive System (RDS)*, Semester thesis, Technische Universität München, Aerospace Department, 2011.

[6] Maughmer, M. and Coder, J., "Comparisons of Theoretical Methods for Predicting Airfoil Aerodynamic Characteristics," Tech. Rep. RDECOM TR 10-D-106, The Pennsylvania State University, Aug. 2010.

[7] Drela, M., "XFOIL: An Analysis and Design System for Low Reynolds Number Airfoils," *Low Reynolds Number Aerodynam-*

ics, edited by T. Müller, Vol. 54 of *Lecture Notes in Engineering*, Springer Berlin Heidelberg, 1989, pp. 1–12.

[8] Ragni, D., Ferreira, C. S. a., and Correale, G., "Experimental investigation of an optimized airfoil for vertical-axis wind turbines," *Wind Energy*, Vol. 18, No. 9, 2015, pp. 1629–1643.

[9] Björck, A., "Coordinates and Calculations for the FFA-Wl-xxx, FFA-W2-xxx and FFA-W3-xxx Series of Airfoils for Horizontal Axis Wind Turbines," Tech. Rep. FFA TN 1990-15, Flygtekniska Försöksanstalten, The Aeronautical Research Institute of Sweden, Aerodynamics Department, 1990.

[10] Somers, D. and Maughmer, M., "Theoretical Aerodynamic Analyses of Six Airfoils for Use on Small Wind Turbines," Tech. Rep. NREL/SR-500-33295, Airfoils, Inc., Port Matilda, Pennsylvania, 2002.

[11] Kintscher, M., Monner, H., and Heintze, O., "Experimental Testing of a Smart Leading Edge High Lift Device for Commercial Transportation Aircrafts," *27th International Congress of the Aeronautical Sciences (ICAS)*, Sept. 2010.

[12] Monner, H. and Kintscher, M., "Design of a Smart Droop Nose as Leading Edge High Lift System for Transportation Aircrafts," *50th AIAA/ASME/ASCE/AHS/ASC Structures, Structural Dynamics, and Materials Conference*, May 2009.

[13] Monner, H., *Erzielung einer optimierten Tragflügelverwölbung durch den Einsatz formvariabler Klappenstrukturen*, Ph.D. dissertation, Institut für Faserverbundleichtbau und Adaptronik, Institut für Strukturmechanik, DLR, 2000.

[14] Monner, H., Sachau, D., and Breitbach, E., "Design Aspects of the Elastic Trailing Edge for an Adaptive Wing," *Research and Technology Agency, Ottawa, Canada*, Oct. 1999.

[15] Thill, C., Etches, J., Bond, I., Potter, K., and Weaver, P., "Morphing skins," *The Aeronautical Journal*, Vol. 112, No. 1129, 2008, pp. 117–139.

[16] Morishima, R., Guo, S., and Ahmed, S., "A Composite Wing with a Morphing Leading Edge," *51st AIAA/ASME/ASCE/AHS/ASC Structures, Structural Dynamics, and Materials Conference*, April 2010.

[17] Molinari, G., Quack, M., Dmitriev, V., Morari, M., Jenny, P., and Ermanni, P., "A Multidisciplinary Approach for Wing Morphing," *21st International Conference on Adaptive Structures and Technologies (ICAST)*, 2010.

[18] Simons, M., *Sailplanes: 1965–2000*, EQIP Werbung & Verlag GmbH, 2004.

[19] Müller, D., *Das Hornkonzept - Realisierung eines formvariablen Tragflügelprofils zur aerodynamischen Leistungsoptimierung zukünftiger Verkehrsflugzeuge*, Ph.D. dissertation, Fakultät Luft- und Raumfahrttechnik, Universität Stuttgart, Jan. 2000.

[20] Kraus, D., *Auslegung einer formvariablen Tragflügelvorderkante eines Hochleistungssegelflugzeugs*, Semester thesis, Technische Universität München, Aerospace Department, Institute of Lightweight Structures, 2013.

[21] Weinzierl, M., *Design der hochelastischen Sektion einer formvariablen Tragflächenvorderkante der Mü 3x Wölbfips*, Semester thesis, Technische Universität München, Aerospace Department, Institute of Lightweight Structures, 2013.

[22] Bubert, E., Woods, B., Lee, K., Kothera, C., and Wereley, N., "Design and Fabrication of a Passive 1D Morphing Aircraft Skin," *Journal of Intelligent Material Systems and Structures*, Vol. 21, No. 17, 2010, pp. 1699–1717.

[23] Olympio, K. R. and Gandhi, F., "Zero Poisson's Ratio Cellular Honeycombs for Flex Skins Undergoing One–Dimensional Morphing," *Journal of Intelligent Material Systems and Structures*, Vol. 21, No. 17, 2010, pp. 1737–1753.

[24] Xu, X., *Morphing skin design for form variable airfoil cambers using a sandwich concepts*, Master's thesis, Technische Universität München, Aerospace Department, Institute of Lightweight Structures, 2012.

[25] Optical Systems, *Material data sheet PA2200*, Dec. 2008.